A_{2A} adenosine receptor functional states characterized by ^{19}F-NMR

Lukas Sušac[a], Matthew T. Eddy[a,b], Tatiana Didenko[a], Raymond C. Stevens[b], and Kurt Wüthrich[a,c,1]

[a]Department of Integrative Structural and Computational Biology, The Scripps Research Institute, La Jolla, CA 92037; [b]The Bridge Institute, Department of Biological Sciences, University of Southern California, Los Angeles, CA 90089; and [c]Skaggs Institute for Chemical Biology, The Scripps Research Institute, La Jolla, CA 92037

Contributed by Kurt Wüthrich, October 11, 2018 (sent for review August 17, 2018; reviewed by Michael F. Summers and David E. Wemmer)

The human proteome contains 826 G protein-coupled receptors (GPCR), which control a wide array of key physiological functions, making them important drug targets. GPCR functions are based on allosteric coupling from the extracellular orthosteric drug binding site across the cell membrane to intracellular binding sites for partners such as G proteins and arrestins. This signaling process is related to dynamic equilibria in conformational ensembles that can be observed by NMR in solution. A previous high-resolution NMR study of the A_{2A} adenosine receptor (A_{2A}AR) resulted in a qualitative characterization of a network of such local polymorphisms. Here, we used ^{19}F-NMR experiments with probes at the A_{2A}AR intracellular surface, which provides the high sensitivity needed for a refined description of different receptor activation states by ensembles of simultaneously populated conformers and the rates of exchange among them. We observed two agonist-stabilized substates that are not measurably populated in apo-A_{2A}AR and one inactive substate that is not seen in complexes with agonists, suggesting that A_{2A}AR activation includes both induced fit and conformational selection mechanisms. Comparison of A_{2A}AR and a constitutively active mutant established relations between the ^{19}F-NMR spectra and signaling activity, which enabled direct assessment of the difference in basal activity between the native protein and its variant.

NMR spectroscopy | GPCR | adenosine receptor | signaling | dynamics

G protein-coupled receptors (GPCRs) are cell surface sensory proteins that recognize a vast array of extracellular stimuli and form signaling complexes with intracellular partner proteins that drive physiological responses. Approximately 35% of all FDA-approved drugs target human GPCRs, and development of new GPCR drugs shows no signs of slowing down (1). Drug development is supported by both 3D structures of GPCRs and GPCR complexes obtained by X-ray crystallography and cryo-EM and by knowledge about their dynamic structural plasticity gained using other biophysical methods such as NMR spectroscopy. NMR in solution possesses the unique ability to observe multiple, simultaneously populated GPCR conformers, establish relations between their populations and the efficacies of bound drugs, and thus provide direct insight into dynamic processes that underlie physiological GPCR signaling.

In this study, we apply ^{19}F-NMR to refine our understanding of signaling mechanisms in the human A_{2A} adenosine receptor (A_{2A}AR). A_{2A}AR functions have been studied in the central nervous system as a key modulator of neurotransmitters (2), in the cardiovascular system as regulating vasodilation (3), and in the immune system as a T-cell surface immune checkpoint protein (4). Correspondingly, A_{2A}AR has been targeted for various diseases, including Parkinson's disease (5) and depression (6), and new drugs are under development for cancer therapies (7, 8). To gain a deeper understanding of A_{2A}AR functionality, X-ray crystal structures have been reported for its complexes with antagonists (9–12) and agonists (13, 14) and for a ternary complex with an agonist and a "mini G protein" (15). The extensive data on structure and function now provide a foundation for other biophysical techniques to provide complementary insights into the signaling mechanisms. Here we used NMR spectroscopy in solution.

In earlier high-resolution NMR studies of stable-isotope–labeled A_{2A}AR, NMR observations afforded a global view of structural plasticity throughout the 3D structure, and changes in conformational equilibria could be related to variable drug efficacies and to inactivation of an allosteric switch (16, 17). To characterize these structure ensembles in greater detail and to quantify rates of exchange among the different conformers, we now used ^{19}F-NMR with single extrinsic probes judiciously placed in positions at the intracellular tips of the transmembrane helices (TM) VI, VII, and VIII. The increased sensitivity of this ^{19}F-NMR approach relative to 2D heteronuclear correlation experiments permitted quantitative measurements of drug efficacy-related changes in the populations of multiple conformers and the exchange rates among them. The results obtained will be placed in context with data collected using different ^{19}F-NMR probes positioned differently in the A_{2A}AR structure (18, 19) and by ^{13}C-methyl NMR of selectively labeled isoleucine residues on a deuterated background (20).

Results

Selecting Locations for ^{19}F-NMR Probes in A_{2A}AR. The chemical reaction used here for the introduction of ^{19}F-groups targets cysteine side chains via a disulfide bond formation. Wild-type

Significance

G protein-coupled receptor (GPCR) signaling from the extracellular orthosteric drug binding site across the cell membrane to the intracellular contact sites with G proteins and arrestins is enabled by inherent structural plasticity, which can be observed by NMR spectroscopy. Here, we use ^{19}F-NMR to characterize ensembles of different, simultaneously populated conformations of the human A_{2A} adenosine receptor in function-related equilibria. The NMR data support an activation model involving both induced fit and reequilibration of conformational ensembles, and experiments with a constitutively active mutant of A_{2A} adenosine receptor (A_{2A}AR) established correlations between NMR parameters and GPCR basal activity. The present quantitative measurements with observation of judiciously engineered ^{19}F-NMR probes complement a previous qualitative overall view of A_{2A}AR dynamics from high-resolution NMR.

Author contributions: L.S., R.C.S., and K.W. designed research; L.S. and T.D. performed the experimental work; L.S., M.T.E., T.D., and K.W. analyzed data; and L.S., M.T.E., T.D., and K.W. wrote the paper.

Reviewers: M.F.S., Howard Hughes Medical Institute, University of Maryland, Baltimore County; and D.E.W., University of California, Berkeley.

The authors declare no conflict of interest.

[1]To whom correspondence should be addressed. Email: wuthrich@scripps.edu.

This article contains supporting information online at www.pnas.org/lookup/suppl/doi:10.1073/pnas.1813649115/-/DCSupplemental.

Published online November 21, 2018.

$A_{A2}AR$ contains 14 cysteines, of which 8 are in disulfide bonds and thus protected from the chemical reagent. In the 3D structure of $A_{A2}AR$, the remaining six cysteine residues are located in the membrane interior and therefore also inaccessible for chemical reagents, provided that the technique of in-membrane chemical modification (IMCM) (21) is used for the introduction of the NMR probes. Without the need for other amino acid replacements, ^{19}F-NMR reporter groups could thus be introduced by design into locations near the intracellular surface, where their possible response to ligand-induced conformational rearrangements can provide insights into the mechanisms enabling the physiological signaling by $A_{A2}AR$. Cys residues were thus engineered into three such locations and then reacted with 2,2,2-trifluoroethanethiol (TET), yielding C^{TET} (22).

The selection of the engineered Cys sites was based on comparison of crystal structures of $A_{2A}AR$ complexes with antagonists and agonists, which showed that the intracellular ends of the transmembrane helices (TM) VI and VII undergo major rearrangements (10–13, 23, 24). We therefore introduced cysteines into sequence positions 225 and 289, which are located near the intracellular tips of TM VI and TM VII, yielding $A_{2A}AR$[L225C] and $A_{2A}AR$[A289C] (Fig. 1 *A* and *B*). In the selection of these two sites, we also considered earlier NMR and crystallographic studies with rhodopsin, the β_2-adrenergic receptor (β_2AR), and $A_{2A}AR$, which had identified similar receptor locations as hotspots for activation-related conformational changes (22, 25–30).

As a control, we also investigated $A_{2A}AR$[R304C^{TET}], where the position of the engineered cysteine in helix VIII does not show major differences between the crystal structures of $A_{2A}AR$ complexes with agonists and antagonists (10, 12–14).

All three variants of $A_{2A}AR$ used here were shown to retain the pharmacological activity of the parent receptor, using radioligand saturation binding (*SI Appendix*, Fig. S1).

The ^{19}F-NMR of $A_{2A}AR$ Complexes Shows Different Conformational Ensembles in Response to Variable Efficacy of the Bound Drug. Experiments with $A_{2A}AR$[A289C^{TET}] revealed pronounced ^{19}F-NMR spectral changes between agonist complexes and antagonist complexes. The complexes with antagonists contain two signals with chemical shifts $\delta \approx 11.4$ ppm (P_3) and $\delta \approx 9.5$ ppm (P_1), which coincides with the spectrum of apo-$A_{2A}AR$[A289C^{TET}] (Fig. 1*C*). Complexes with agonists contain a signal at the chemical shift of P_1 and two new signals, P_2 and P_4, at $\delta \approx$ 10.8 and 13.1 ppm, but there is no signal intensity at position P_3 (Fig. 1*C*). The line shapes of the dominant components in the spectra of antagonist and agonist complexes at 9.5 and 11.4 ppm, respectively, are closely similar and narrower than the other components. There are at most subtle variations among the spectra of complexes with different antagonists or with different agonists (*SI Appendix*, Table S1), respectively (Fig. 1 and *SI Appendix*, Fig. S2), so that the ^{19}F-NMR spectra of $A_{2A}AR$[A289C^{TET}] represent "fingerprints" for the corresponding functional states. The two different patterns of ^{19}F-NMR signals seen in Fig. 1*C* are thus characteristic of conformational ensembles associated, respectively, with the functionally inactive receptor and its active-like state present when an agonist is bound to the extracellular orthosteric site in the absence of interactions with intracellular partner proteins. This assignment is further supported by the ^{19}F-NMR–detected ligand competition experiments of Fig. 1*D*. Starting with the two-signal spectrum of apo-$A_{2A}AR$[A289C^{TET}], addition of the agonist NECA resulted in the appearance of the characteristic spectral features for agonist complexes. Subsequent addition of an excess of the high-affinity antagonist ZM241385 yielded a spectrum characteristic of the antagonist-bound receptor. We conclude that we observed transitions from an inactive conformational ensemble of apo-$A_{2A}AR$[A289C^{TET}] to an active-like ensemble of the complex with NECA and then from this active-like state to an inactive ensemble of the complex with ZM241385. It is intriguing that the complex of $A_{2A}AR$ with the partial agonist LUF 5834 shows the signal of the inactive

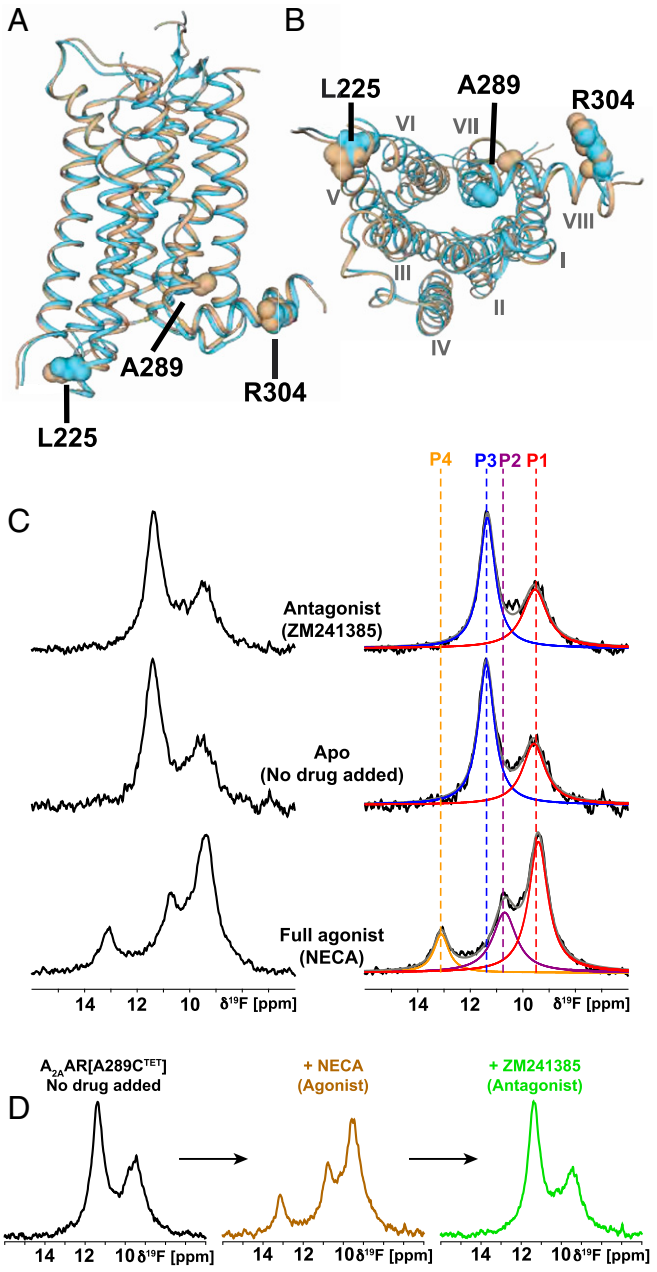

Fig. 1. Location of ^{19}F-NMR probes in the crystal structure of $A_{2A}AR$ and NMR response to variable drug efficacy. (*A*) Side view of a superposition of the antagonist complex $A_{2A}AR$–ZM241385 (brown, PDB-ID: 3ELM) with the agonist complex $A_{2A}AR$–UK432097 (cyan, PDB-ID: 3QAK); the extracellular membrane surface is at the top. The three sequence positions selected for the ^{19}F labels are highlighted by spheres and identified. (*B*) Same as *A*, view onto the intracellular surface; Roman numerals indicate the TM numbering. (*C*) The 1D ^{19}F-NMR spectra of $A_{2A}AR$[A289C^{TET}] complexes with ligands of varying efficacy, as indicated in the *Center*. On the *Right*, the NMR spectra shown on the *Left* are interpreted by Lorentzian deconvolutions with the minimal number of components that provided a good fit, i.e., P_1 to P_4. The chemical shift positions of P_1 to P_4 are indicated by colored broken vertical lines. (*D*) The 1D ^{19}F-NMR observation of ligand exchange in $A_{2A}AR$[A289C^{TET}]. The agonist NECA was added at saturating concentration to the apo-$A_{2A}AR$ and then displaced by the more strongly binding antagonist ZM241385.

state, rather than that for the active-like state (Fig. 1 and *SI Appendix*, Fig. S2).

Observation of the ^{19}F-NMR signals originating from C^{TET} in sequence position 225 provided similar results to those obtained from observation of C^{TET} in position 289. Despite the much smaller dispersion of the chemical shifts (see also the next section), the presence of a new signal for complexes of $A_{2A}AR$ [$L225C^{TET}$] with agonists, compared with complexes with antagonists, is readily apparent (*SI Appendix*, Fig. S3). The signals obtained from the reporter group in position 225 are again identical among different antagonist complexes and the apo-form of the receptor, and different agonist complexes also show closely similar ^{19}F-NMR signals (*SI Appendix*, Fig. S3). Deconvolution of the signals showed a good fit with the assumption of two and three components for the inactive and active-like states (*SI Appendix*, Fig. S3). While the relative intensities and line widths assigned to the two components of the inactive state signal coincide qualitatively with those observed at $C^{TET}289$, the intensity distributions in the signals for the active-like states is clearly different, indicating different responses to drug efficacy at the tips of TMVI and TMVII.

For C^{TET} in sequence position 304, no differences were seen between the ^{19}F-NMR signals of the apo-form, complexes with antagonists, and complexes with agonists (*SI Appendix*, Fig. S4). This absence of a response to different efficacies of the bound ligand is in line with the absence of differences in the spatial arrangement of helix VIII between crystal structures of $A_{2A}AR$ complexes with agonists or antagonists (Fig. 1 *A* and *B*).

In the continuation of this work, we focus on drug complexes with $A_{2A}AR[A289C^{TET}]$, making use of the high spectral resolution of the ^{19}F-NMR spectra recorded with this probe location.

The ^{19}F-NMR in Solution and Crystal Structures of $A_{2A}AR$. To link the NMR data with the available $A_{2A}AR$ crystal structures, we performed aromatic ring current shift (δ_R) calculations (*SI Appendix*, Table S2) (31, 32). Since only small ring current shifts of <0.1 ppm were calculated for the C^{TET} groups at positions 225 and 304, which is due to the absence of nearby aromatic residues and consistent with the small chemical shift dispersion observed at these two sites (*SI Appendix*, Figs. S3 and S4), the following discussion is focused on $A_{2A}AR$ [$A289C^{TET}$]. For the $A_{2A}AR$–ZM214385 complex, a small downfield shift of $\delta_R \approx 0.2$ ppm was calculated, and for $A_{2A}AR$–NECA there was a large upfield shift of $\delta_R \approx -1.4$ ppm. The difference of about 1.6 ppm is due to conformational rearrangements that bring the aromatic rings of Phe286, Phe295, and Phe299 into proximity of residue 289 in the structure of the agonist complex. These calculated shifts are in close agreement with the experimental chemical shift difference of 1.9 ppm between signals P_1 and P_3 (Fig. 1*C*), whereas all other combinations of pairs of possible corresponding peaks in the two spectra do not fit the crystal data. The implication is that the most highly populated states P_3 and P_1 in the complexes with ZM241385 and NECA, respectively, coincide with the corresponding crystal structures, whereas the conformers giving rise to the NMR signal P_1 in the antagonist complex and those represented by P_2 and P_4 in the agonist complex were not seen in the crystals. Additional ring current calculations using the presumed fully active state in the crystal structure of the ternary complex of $A_{2A}AR$, NECA, and a "mini G protein" (15) yielded an upfield shift of $\delta_R \approx -1.2$ ppm for Ala289, which is close to that for the active-like $A_{2A}AR$–NECA state. In summary, the ring current calculations yielded assignments for the dominantly populated conformations of the inactive (P_3) and active-like (P_1) states and support that the crystal structures do not represent the full repertoire of $A_{2A}AR$ conformations present in solution at ambient temperature.

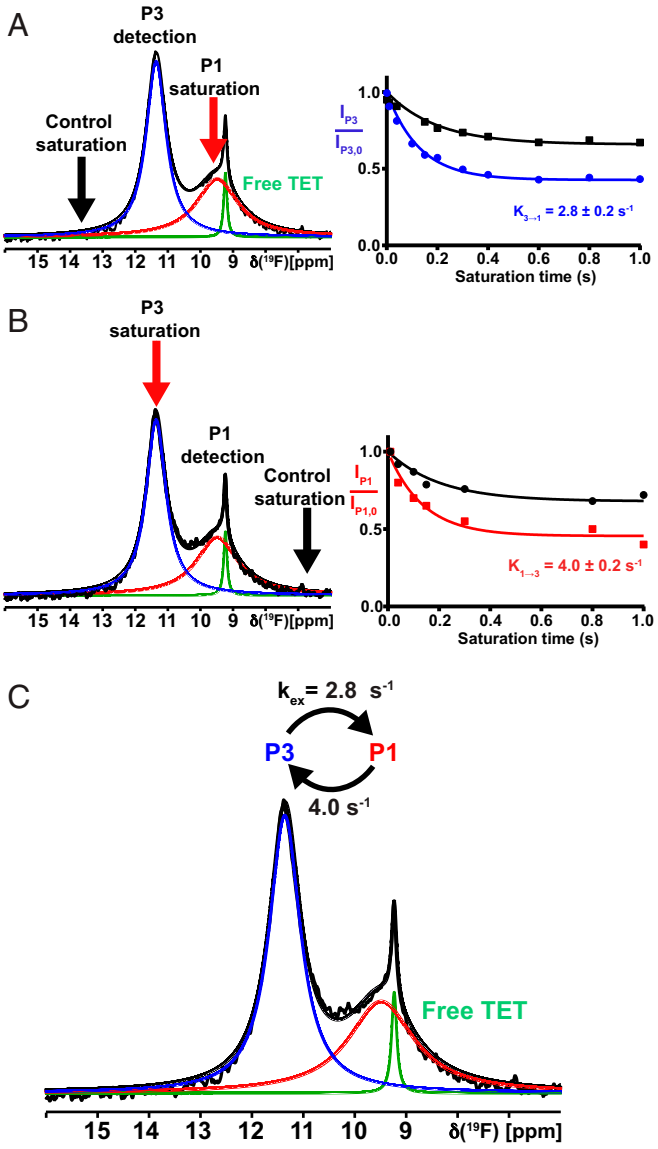

Fig. 2. Conformational exchange in the $A_{2A}AR$ complex with the antagonist ZM241385 by ^{19}F-NMR saturation transfer. (*A*, *Left*) The 1D ^{19}F-NMR spectrum. The Lorentzian deconvolution introduced in Fig. 1 is indicated. A red arrow indicates the carrier position for the preirradiation, and a black arrow indicates the position for the reference measurement. The observed peak is indicated by "detection." (*A*, *Right*) Plots of the normalized intensity of the observed peak, P_3, versus the saturation pulse length after irradiation on P_1 (cyan) and at the control (black). (*B*) Same as *A*, with inverted direction. (*C*) Survey of the conformational exchange rates in the $A_{2A}AR[A289C^{TET}]$–ZM241385 complex.

Rate Processes in Function-Related Conformational Ensembles of $A_{2A}AR$. The presence of individually resolved NMR signals establishes an upper limit for the exchange rates (k_{ex}) between the $A_{2A}AR$ conformations represented by these signals, i.e., $k_{ex} \lesssim 10^{-3}$ s^{-1}. Here, we explore the dynamic processes in these conformational ensembles further with saturation transfer difference experiments (STD) (33, 34) and 2D exchange spectroscopy (EXSY) (35).

For the $A_{2A}AR$[A289C]–ZM241385 complex, 1D ^{19}F-STD experiments were performed with preirradiation on P_1, monitoring changes in the intensity of P_3, and collecting reference data with preirradiation at 13.3 ppm. The saturation times were 0.05–1.0 s. The measurements were then performed also with preirradiation at P_3 and detection on P_1 (Fig. 2 *A* and *B*).

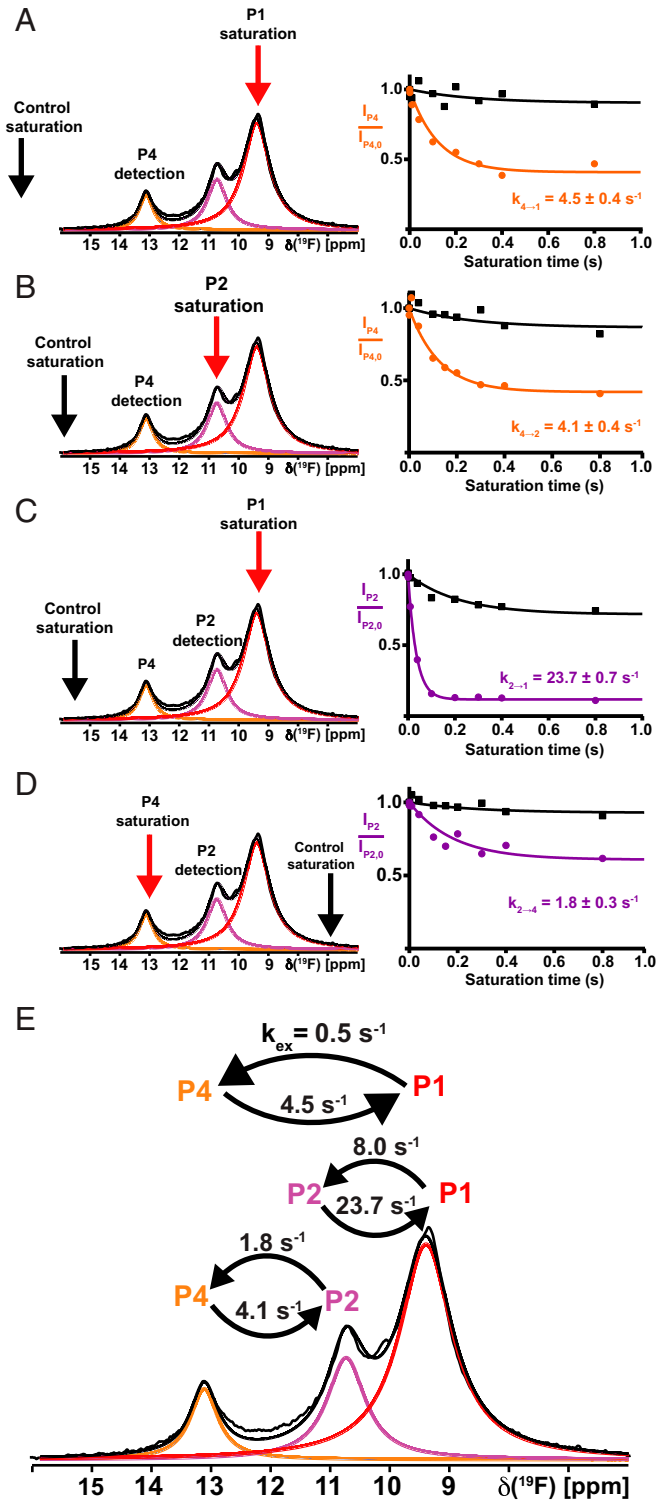

Fig. 3. Conformational exchange in the $A_{2A}AR$ complex with the full agonist NECA by ^{19}F-NMR saturation transfer. (*A–D*) Four individual measurements linking P_1, P_2, and P_4, same presentation as in Fig. 2 *A* and *B*. (*E*) Survey of the conformational exchange rates in the $A_{2A}AR[A289C^{TET}]$–NECA complex. Please note in *C* and *D* that the saturation and control saturation are not symmetrical to the detection position, and this arrangement was chosen to prevent falsification of the data by direct irradiation of the tail of the observed signal.

Analysis of the STD data using the Bloch–McConnell formalism (36, 37) established that k_{ex} (3→1) = 2.8 s^{-1} and k_{ex} (1→3) = 4.0 s^{-1} (Fig. 2*C*).

For agonist-bound $A_{2A}AR[A289C^{TET}]$, STD experiments were performed with preirradiation of all three signals (Fig. 3 *A–D*, red arrows), and reference data were recorded with preirradiation at the chemical shifts indicated by the black arrows in the figure. Analysis of the STD data resulted in the following exchange rates: k_{ex} (4→1) = 4.5 s^{-1}, k_{ex} (1→4) = 0.5 s^{-1}, k_{ex} (4→2) = 4.1 s^{-1}, k_{ex} (2→4) = 1.8 s^{-1}, k_{ex} (2→1) = 23.7 s^{-1}, and k_{ex} (1→2) = 8.0 s^{-1} (Fig. 3*E*). It is remarkable that with the exception of k_{ex} (2→1) and k_{ex} (1→2), slow exchange was measured for all pairs of conformers.

The conformational exchange rates from STD measurements were qualitatively confirmed with the use of 2D exchange spectroscopy (EXSY). In the 2D [^{19}F,^{19}F]-EXSY spectrum of the $A_{2A}AR[A289C^{TET}]$ complex with the agonist NECA, exchange crosspeaks between P_2 and P_1 were observed, but there were no crosspeaks between P_4 and either P_1 or P_2 (Fig. 4). There were no crosspeaks between the two NMR signals of the antagonist-bound receptor (Fig. 1). The EXSY data thus confirm the coexistence of widely different exchange rates among the conformational substates of the different activation levels of $A_{2A}AR$ (Figs. 2*C* and 3*E*).

The ^{19}F-NMR–Based Comparison of $A_{2A}AR$ with a Constitutively Active Variant. $A_{2A}AR[S91A]$, which contains a single amino acid replacement near the allosteric switch at $D^{2.50}$ in the transmembrane-spanning region of the receptor, has been demonstrated to exhibit significant basal activity and increased signaling at full activation in HEK293T cells stimulated with the full agonist CGS21680 (38). The ^{19}F-NMR spectra of $A_{2A}AR[S91A, A289C^{TET}]$ show qualitatively similar signals and exchange rates as $A_{2A}AR$ (*SI Appendix*, Fig. S5), confirming the structural integrity of the modified protein. Nonetheless, the functional differences relative to $A_{2A}AR$ are paralleled by important differences between the NMR spectra. The apo-form of the variant protein shows increased intensity for the signal P_1, compared with apo-$A_{2A}AR[A289C^{TET}]$, and there is a weak peak at the position P_4, which had no signal intensity in apo-$A_{2A}AR$. Upon addition of the agonist NECA, spectra of $A_{2A}AR[S91A, A289C^{TET}]$ showed increased intensities for the signals P_1 and P_4, compared with $A_{2A}AR[A289C^{TET}]$, where the increased intensity of P_4 was particularly striking. In competition binding experiments, addition of an excess amount of the high-affinity antagonist ZM241385 to the NECA-bound $A_{2A}AR[S91A, A289C^{TET}]$ yielded a spectrum with similar signal positions as for the apo-protein, but different relative

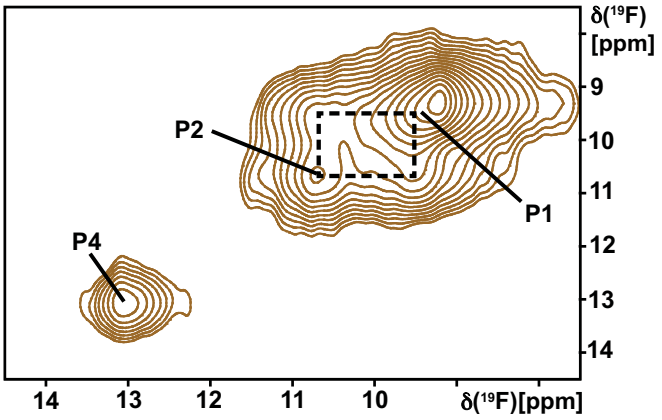

Fig. 4. Conformational exchange in the $A_{2A}AR$ complex with the full agonist NECA observed by 2D exchange spectroscopy. A contour plot is shown of a 2D [^{19}F, ^{19}F]-EXSY spectrum collected at 280 K with a mixing time of 100 ms. The diagonal peak positions of P_1, P_2, and P_4 are labeled, and a dashed box indicates crosspeaks observed between P_1 and P_2.

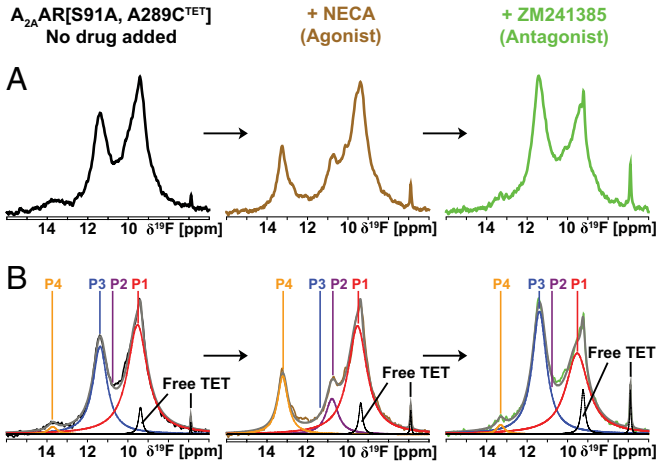

Fig. 5. Dynamic processes in the ^{19}F-labeled constitutively active mutant A_{2A}AR[S91A, A289C^{TET}] observed by 1D ^{19}F-NMR. (*A*) Same ligand exchange experiment as in Fig. 1*D*. (*B*) Lorentzian deconvolutions of the spectra shown in *A*.

signal intensities (Fig. 5*B*). Overall, in contrast to A_{2A}AR, the spectra of the apo-form and the antagonist-bound complex of the constitutively active mutant protein contain admixtures of ^{19}F-NMR signals that are characteristic of the active-like state. For both the inactive state and active-like state, the exchange rates among the different conformers represented by the individual ^{19}F-NMR signals are closely similar to those measured for the wild-type protein (Figs. 2 and 3 and *SI Appendix*, Fig. S5).

Discussion

The present quantitative description of A_{2A}AR structural ensembles by ^{19}F-NMR probes complements a recent qualitative many-parameter overview of A_{2A}AR structural plasticity by high-resolution NMR, which revealed that there are structural manifolds linked to function (16, 17). The ^{19}F-NMR spectra observed for probes in TM VI and TM VII are qualitatively similar, but only the spectra TM VII are sufficiently well resolved to enable quantitative measurements, due to the location of the $-CF_3$ group near aromatic residues that reflect the efficacy of bound drugs.

The STD and 2D EXSY (Figs. 2–4) showed that exchange between the two conformers of the inactive state and with the component P4 in the active-like state is slow. The corresponding high energy barrier indicates that differences between these substates likely involve major structural rearrangements of the polypeptide backbone, while the active-like state contains also two substates, P_2 and P_1 (Figs. 3 and 4), with a low energy barrier for interconversion. The available data indicate that all substates of the active-like conformation are separated from the inactive state by high energy barriers.

Overall, two conclusions can be drawn from the observations. First, considering the high energy barriers separating at least one component in each activation state from the other structures in the ensemble, it could be that only one of the conformers is linked to activation. Second, the difference in resolution between the probes on TM VI and TM VII (Fig. 1 and *SI Appendix*, Fig. S3) illustrates how the NMR data can be optimized by placement of probes near indigenous aromatic amino acid residues, or possibly by introduction of extrinsic aromatic residues near the NMR probe (39).

A_{2A}AR is the second human GPCR studied by ^{19}F-NMR in solution, after the β_2-adrenergic receptor (β_2AR), which contained equilibria between one inactive conformational state and one active-like state (26), which were in slow exchange (25) and showed different relative populations at different probe sites. Considering the present data for A_{2A}AR, we conclude that β_2AR cannot serve as a model for human GPCRs overall, or even for class A GPCRs. It is further intriguing that the relative populations of active-like states in β_2AR could be directly related to biased agonism (26). Since there are no published findings of biased agonists for A_{2A}AR, ^{19}F-NMR experiments may guide future efforts to explore A_{2A}AR biased agonists.

Since the intensity of the NMR signal P_4 of agonist-bound A_{2A}AR could be related to the activation level, it now provides a means for assessing basal activity (Fig. 6). As no admixtures of active-like states were detected in either apo- or antagonist-bound A_{2A}AR[A289C^{TET}] (Fig. 1 *C* and *D*), we conclude that the ^{19}F-NMR data reflect the inherently low basal activity of A_{2A}AR measured in cells (38). Recent NMR studies using a ^{19}F probe in a position on helix VI, which provided a limited chemical shift dispersion comparable to the one shown in *SI Appendix*, Fig. S3, was interpreted to show that the basal activity amounted to 70% of the activity of agonist-bound A_{2A}AR (18, 19). Clearly, this contrasts with the present NMR studies and with literature data of the pharmalogical activity of A_{2A}AR (38). There are additional apparent discrepancies in refs. 18 and 19 relative to the present data; in view of the large chemical shift dispersion and the resulting high spectral resolution by our ^{19}F probe, we are confident in the interpretation of our results.

From the relations between the ^{19}F-NMR data and the A_{2A}AR crystal structures revealed by ring current shift calculations (*SI Appendix*, Table S2), only one combination of substates between inactive and active-like A_{2A}AR is consistent with predicted chemical shifts from the crystal structures. This pair of substates is dominantly populated and shows narrower NMR lines than all other substates except for P4 (Fig. 1). The NMR data in solution at ambient temperature thus manifest conformations that are not observed in crystals. This is most apparent for signal P_4, which is shifted downfield by ~1.5 ppm from the predicted chemical shift for the active-like state. The increased intensity of the NMR signal P_4 for the antagonist complex of a constitutively active mutant establishes a direct relation to A_{2A}AR activation. Since all available A_{2A}AR crystal structures thus represent only a fraction of the repertoire of function-relevant conformations, it could even be that the physiological action of A_{2A}AR is mainly based on a conformer that has not yet been seen in crystal structures. In this context, it is also intriguing that A_{2A}AR[A289C^{TET}] with the bound partial agonist LUF5834 yields spectra that are those of antagonist-bound

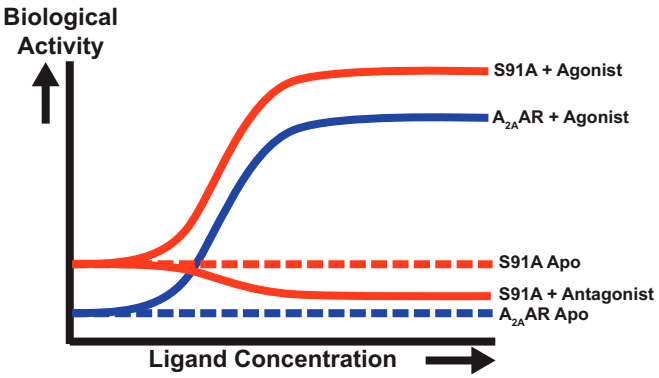

Fig. 6. Biological response versus ligand concentration as manifested in the ^{19}F NMR spectra. A plot is shown of the biological activity (i.e., G protein signaling) versus ligand concentration for A_{2A}AR and A_{2A}AR [S91A], as labeled on the right of the individual sigmoidal response curves. Relative biological activity was determined by observation of the intensity of the peak P_4 in ^{19}F-NMR spectra of A_{2A}AR[A289C^{TET}] and A_{2A}AR[S91A, A289C^{TET}]. The dashed lines represent the basal signaling level of the two proteins.

$A_{2A}AR[A289C^{TET}]$, which suggests that the local conformation at the intracellular end of TM VII corresponds to an inactive state for this partial agonist.

Materials and Methods

The TET-labeled $A_{2A}AR$ variants used in this study were expressed and purified as previously described (21). The solutions used for NMR measurements contained 25 to 50 μM protein in 50 mM Hepes at pH 7.5, 150 mM NaCl, 0.05% DDM, 0.01% CHS, and excess ligand. All NMR data were measured on a Bruker AVANCE 600 spectrometer using a QCI $^{1}H/^{19}F$-$^{13}C/^{15}N$ quadruple resonance cryoprobe with shielded *z*-gradient coil. Spectra were processed using Bruker TOPSPIN version 3.1, and signals were deconvoluted using the MNOVA software version 10.0.0.2. Additional details are described in *SI Appendix*.

ACKNOWLEDGMENTS. The authors thank K. White (University of Southern California) for help with analysis of the radioligand binding dating. We acknowledge support from the NIH/National Institute of General Medical Sciences (Protein Structure Initiative Biology Grants U54 GM094618 and R01GM115825). L.S. was supported by a Boehringer Ingelheim Fonds PhD fellowship and by the German Academic Exchange Service (DAAD). M.T.E. acknowledges an American Cancer Society postdoctoral research fellowship. K.W. is the Cecil H. and Ida M. Green Professor of Structural Biology at The Scripps Research Institute.

1. Hauser AS, Attwood MM, Rask-Andersen M, Schiöth HB, Gloriam DE (2017) Trends in GPCR drug discovery: New agents, targets and indications. *Nat Rev Drug Discov* 16: 829–842.
2. Fredholm BB, Chen J-F, Masino SA, Vaugeois J-M (2005) Actions of adenosine at its receptors in the CNS: Insights from knockouts and drugs. *Annu Rev Pharmacol Toxicol* 45:385–412.
3. Belardinelli L, et al. (1998) The A2A adenosine receptor mediates coronary vasodilation. *J Pharmacol Exp Ther* 284:1066–1073.
4. Jacobson KA, Gao Z-G (2006) Adenosine receptors as therapeutic targets. *Nat Rev Drug Discov* 5:247–264.
5. Armentero MT, et al. (2011) Past, present and future of A(2A) adenosine receptor antagonists in the therapy of Parkinson's disease. *Pharmacol Ther* 132:280–299.
6. Collins LE, et al. (2012) The novel adenosine A2A antagonist Lu AA47070 reverses the motor and motivational effects produced by dopamine D2 receptor blockade. *Pharmacol Biochem Behav* 100:498–505.
7. Young A, et al. (2016) Co-inhibition of CD73 and A2AR adenosine signaling improves anti-tumor immune responses. *Cancer Cell* 30:391–403.
8. Mittal D, et al. (2014) Antimetastatic effects of blocking PD-1 and the adenosine A2A receptor. *Cancer Res* 74:3652–3658.
9. Sun B, et al. (2017) Crystal structure of the adenosine A_{2A} receptor bound to an antagonist reveals a potential allosteric pocket. *Proc Natl Acad Sci USA* 114:2066–2071.
10. Jaakola V-P, et al. (2008) The 2.6 angstrom crystal structure of a human A_{2A} adenosine receptor bound to an antagonist. *Science* 322:1211–1217.
11. White KL, et al. (2018) Structural connection between activation microswitch and allosteric sodium site in GPCR signaling. *Structure* 26:259–269.e5.
12. Doré AS, et al. (2011) Structure of the adenosine A(2A) receptor in complex with ZM241385 and the xanthines XAC and caffeine. *Structure* 19:1283–1293.
13. Xu F, et al. (2011) Structure of an agonist-bound human A_{2A} adenosine receptor. *Science* 332:322–327.
14. Lebon G, et al. (2011) Agonist-bound adenosine A2A receptor structures reveal common features of GPCR activation. *Nature* 474:521–525.
15. Carpenter B, Nehmé R, Warne T, Leslie AGW, Tate CG (2016) Structure of the adenosine A_{2A} receptor bound to an engineered G protein. *Nature* 536:104–107, and erratum (2016) 538:542.
16. Eddy MT, et al. (2018) Extrinsic tryptophans as NMR probes of allosteric coupling in membrane proteins: Application to the A2A adenosine receptor. *J Am Chem Soc* 140: 8228–8235.
17. Eddy MT, et al. (2018) Allosteric coupling of drug binding and intracellular signaling in the A2A adenosine receptor. *Cell* 172:68–80.e12.
18. Ye L, et al. (2018) Mechanistic insights into allosteric regulation of the A_{2A} adenosine G protein-coupled receptor by physiological cations. *Nat Commun* 9:1372.
19. Ye L, Van Eps N, Zimmer M, Ernst OP, Prosser RS (2016) Activation of the A_{2A} adenosine G-protein-coupled receptor by conformational selection. *Nature* 533:265–268.
20. Clark LD, et al. (2017) Ligand modulation of sidechain dynamics in a wild-type human GPCR. *eLife* 6:e28505.
21. Sušac L, O'Connor C, Stevens RC, Wüthrich K (2015) In-membrane chemical modification (IMCM) for site-specific chromophore labeling of GPCRs. *Angew Chem Int Ed Engl* 54:15246–15249.
22. Klein-Seetharaman J, Getmanova EV, Loewen MC, Reeves PJ, Khorana HG (1999) NMR spectroscopy in studies of light-induced structural changes in mammalian rhodopsin: Applicability of solution (19)F NMR. *Proc Natl Acad Sci USA* 96:13744–13749.
23. Hino T, et al. (2012) G-protein-coupled receptor inactivation by an allosteric inverse-agonist antibody. *Nature* 482:237–240.
24. Lebon G, Edwards PC, Leslie AGW, Tate CG (2015) Molecular determinants of CGS21680 binding to the human adenosine A2A receptor. *Mol Pharmacol* 87: 907–915.
25. Horst R, Liu JJ, Stevens RC, Wüthrich K (2013) β_2-adrenergic receptor activation by agonists studied with ^{19}F NMR spectroscopy. *Angew Chem Int Ed Engl* 52:10762–10765.
26. Liu JJ, Horst R, Katritch V, Stevens RC, Wüthrich K (2012) Biased signaling pathways in β_2-adrenergic receptor characterized by 19F-NMR. *Science* 335:1106–1110.
27. Eddy MT, Didenko T, Stevens RC, Wüthrich K (2016) β_2-adrenergic receptor conformational response to fusion protein in the third intracellular loop. *Structure* 24: 2190–2197.
28. Chung KY, et al. (2012) Role of detergents in conformational exchange of a G protein-coupled receptor. *J Biol Chem* 287:36305–36311.
29. Manglik A, et al. (2015) Structural insights into the dynamic process of β2-adrenergic receptor signaling. *Cell* 161:1101–1111.
30. Kim TH, et al. (2013) The role of ligands on the equilibria between functional states of a G protein-coupled receptor. *J Am Chem Soc* 135:9465–9474.
31. Koradi R, Billeter M, Wüthrich K (1996) MOLMOL: A program for display and analysis of macromolecular structures. *J Mol Graph* 14:51–55.
32. Johnson C, Jr, Bovey F (1958) Calculation of nuclear magnetic resonance spectra of aromatic hydrocarbons. *J Phys Chem* 29:1012–1014.
33. Forsen S, Hoffman RA (1964) Exchange rates by nuclear magnetic multiple resonance. III. Exchange reactions in systems with several nonequivalent sites. *J Phys Chem* 40: 1189–1196.
34. Forsén S, Hoffman RA (1963) Study of moderately rapid chemical exchange reactions by means of nuclear magnetic double resonance. *J Phys Chem* 39:2892–2901.
35. Jeener J, Meier BH, Bachmann P, Ernst RR (1979) Investigation of exchange processes by two-dimensional NMR spectroscopy. *J Phys Chem* 71:4546–4553.
36. McConnell HM (1958) Reaction rates by nuclear magnetic resonance. *J Phys Chem* 28: 430–431.
37. Bloch F (1946) Nuclear induction. *Phys Rev* 70:460–474.
38. Massink A, et al. (2015) Sodium ion binding pocket mutations and adenosine A2A receptor function. *Mol Pharmacol* 87:305–313.
39. Liu D, Wüthrich K (2016) Ring current shifts in (19)F-NMR of membrane proteins. *J Biomol NMR* 65:1–5.